Kinetic investigations of nonlinear electrostatic excitations in quantum plasmas

Tian-Xing Hu, Jiong-Hang Liang, and Zheng-Mao Sheng*
Institute for Fusion Theory and Simulation, School of Physics, Zhejiang University, Hangzhou 310027, China

Dong Wu†
Key Laboratory for Laser Plasmas and School of Physics and Astronomy, Collaborative Innovation Center of IFSA, Shanghai Jiao Tong University, Shanghai 200240, China

(Received 18 April 2022; accepted 18 May 2022; published 9 June 2022)

For plasmas in an extremely high-density state, like stellar cores or compressed fuel in inertial fusion facilities, their behavior turns out to be quite different when compared with those plasmas in interstellar space or magnetic confinement devices. To figure out those differences and uncover the kinetic physics in electrostatic excitations, a quantum kinetic code solving Wigner-Poisson equations has been developed. Basic plasmon decay, Landau damping, and two-stream instability of extremely high-density plasmas are investigated by using our newly developed code. Numerical simulations show that in the linear region, the dispersion relations of intrinsic modes can be significantly affected by quantum effects, and such simulation results can be well described by the existing analytical theory. Especially in the nonlinear region, since the space-time scale of collective modes of plasmas is comparable to the electron de Broglie wavelength, their couplings produce some new physics: the energy exchange between the electron and the collective mode results in an abnormal oscillation that does not exist in classical plasmas.

DOI: 10.1103/PhysRevE.105.065203

I. INTRODUCTION

When a plasma is dense enough that the average distance among electrons is comparable to or even smaller than their thermal de Broglie wavelength, the plasma then enters into the quantum regime [1]. Quantum plasmas are also widely existent in the universe. The study of quantum plasma is of great significance in many different fields of physics, such as inertial confinement fusion (ICF) [2], nanophysics [3], astrophysical plasmas [4,5], and warm dense matter (WDM) [6]. Quantum plasma differs from regular plasma in the following two aspects: (i) the equilibrium state of quantum plasma obeys Fermi-Dirac statistics instead of Maxwellian statistics because of the overlapping of electron spatial wave functions; (ii) the quantum wave effect of a single electron alters the collective behavior of quantum plasma since the quantum wave and the plasma wave have a comparable space-time scale.

The state-of-the-art approaches for investigating quantum plasmas are those based on density-functional theory (DFT) [7,8]. The DFT-based methods are often combined with the molecular-dynamics (MD) method or the quantum Monte Carlo (QMC) method [9–11] in order to achieve desirable accuracy in a variety of parameter regions. However, the DFT-based methods usually focus on the microscopic structure of matter, for example the lattice of solids or the shape of molecules, and they only involve a small number of particles (ranging from hundreds to thousands). Therefore, these methods are not suitable for macroscopic or mesoscopic systems in which the number of particles is almost uncountable.

To investigate a macroscopic or a mesoscopic system, a statistical method is often needed. The most popular simulation method in the plasma physics community is the kinetic method. In classical plasmas, the Vlasov equation is often used, with the distribution function determined by spatial position and velocity. However, in quantum mechanics, the coordinate and the velocity of a particle cannot be determined simultaneously due to the uncertainty principle. Hence, a particle with a definite phase space coordinate is ill-defined in a quantum-mechanical system. Nevertheless, the quantum kinetic method with Wigner's quasidistribution function [12] and the Wigner equation [13] enable us to bypass this obstacle.

The quantum kinetic theory (QKT) starts from the second-quantized many-body quantum theory, which converts the equation of motion of the quantum field operator into a Boltzmann-like transport equation, with interactions beyond the Hartree mean-field approximation included in the collisional term [13–15]. Hence, QKT is of great potential in calculating high-order quantum correlations [16]. Nevertheless, the short-range collisional effects are neglected throughout this paper. The importance of collisional effects in classical dense plasma is discussed in, e.g., Ref. [17]. Furthermore, Ref. [18] takes the Pauli exclusion principle into account in order to simulate the degenerate plasmas.

Analogous to the fluid description in classical plasma [19], quantum hydrodynamics (QHD) treats the quantum electron gas as a fluid [19]. The equations of motion of the quantum fluid can be simplified into a single nonlinear Schrödinger

*zmsheng@zju.edu.cn
†dwu.phys@sjtu.edu.cn

equation. Although the QHD is less cumbersome, and in the past two decades a lot of work has been done by using QHD [20–23], its accuracy has yet to be tested [24,25].

In this paper, we take the collisionless quantum kinetic equation, i.e., the Wigner equation [13], as a starting point to investigate the quantum nature of dense plasma. The ions are assumed to be static and serve as a neutralization background throughout this paper. A modified numerical method is adopted. Theory and numerical simulations show that even in the linear region, the dispersion relations of intrinsic modes can be significantly affected by quantum effects. Especially in the nonlinear region, since the space-time scale of collective modes of plasmas is comparable to the electron de Broglie wavelength, their couplings produce some new physics [26]. For example, a single-particle quantum-oscillator-like structure is found in a quantum BGK equilibrium, i.e., a static solution of the nonlinear Wigner equation. Furthermore, energy exchange between the electron and the collective mode result in an abnormal oscillation that does not exist in classical plasmas.

This paper is organized as follows. In Sec. II, we briefly review the basic ideas of QKT, and then our numerical method is brief introduced. Section III displays the basic plasmon decay and quantum Landau damping in the linear region. In Sec. IV, the nonlinear evolution of a quantum two-stream instability is studied in detail.

II. METHODS

A. Description of quantum plasmas

First, it is natural to define a general normalized Planck constant (NPC):

$$\hat{\hbar}_c = \frac{\hbar\omega_p}{m v_c^2}, \tag{1}$$

where m is the electron mass, and v_c stands for a critical velocity of the physical system. For example, if we choose Fermi or thermal velocity as the critical velocity, we have

$$\hat{\hbar}_F = \frac{\hbar\omega_p}{2\mathcal{E}_F}, \quad \hat{\hbar}_T = \frac{\hbar\omega_p}{2k_B T}, \tag{2}$$

respectively. Here, $k_B T$ is the thermal energy of electrons, $\omega_p = \sqrt{4\pi n e^2/m}$ is the plasma frequency, and the Fermi energy $\mathcal{E}_F = \hbar^2(3\pi^2 n)^{2/3}/2m_e$ is the chemical potential of a degenerate zero-temperature electron gas. Notice that these two NPCs are related by the degeneracy of the system:

$$\Theta = \frac{\hat{\hbar}_F}{\hat{\hbar}_T} = \frac{k_B T}{\mathcal{E}_F}, \tag{3}$$

$\hat{\hbar}_F$ is only a function of density:

$$\hat{\hbar}_F = 5.09 \times 10^3 \ \mathrm{cm}^{-\frac{1}{2}} n^{-\frac{1}{6}}, \tag{4}$$

and $\hat{\hbar}_T$ is suitable for situations in which the temperature is high enough to disguise the Fermi statistic effect while the quantum effect still exists to some extent. Another famous pair of characteristic parameters is

$$\Gamma_F = \frac{e^2 n^{\frac{1}{3}}}{\mathcal{E}_F}, \quad \Gamma_T = \frac{e^2 n^{\frac{1}{3}}}{k_B T}. \tag{5}$$

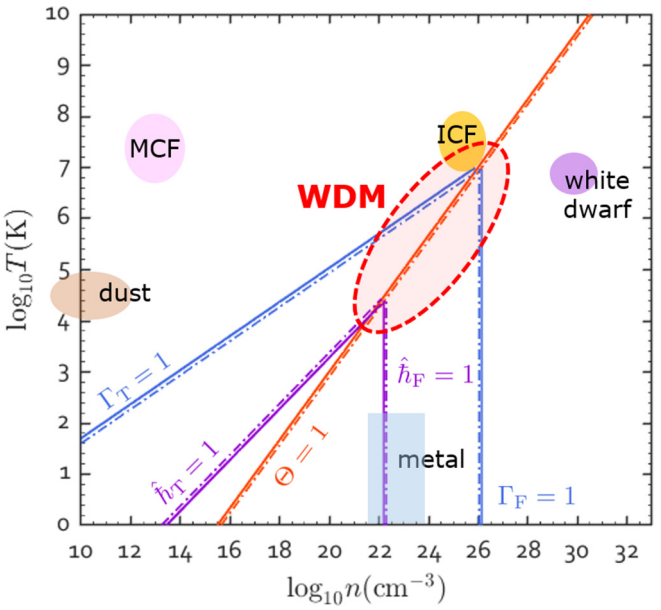

FIG. 1. Relation among different characteristic parameters of quantum plasmas. Each contour consists of a solid line and a dotted line, with the parameter of the region on the side of the solid line being greater than 1, and the parameter on the side of the dotted line being less than 1 [6].

They are the ratio between Coulomb potential energy and Fermi/thermal energy. The traces of characteristic parameters mentioned above equal to 1 are plotted in Fig. 1, from which one can see that $\Theta = \hat{\hbar}_F = \hat{\hbar}_T = 1$ stands for a low-density–low-temperature WDM, and $\Theta = \Gamma_F = \Gamma_T = 1$ denotes a high-density–high-temperature WDM.

The velocity distribution obeys the Fermi-Dirac statistics:

$$f_{FD3}(v) = \frac{3n}{4\pi} \frac{1}{e^{(v^2-\hat{\mu})/\Theta} + 1}, \tag{6}$$

where $\hat{\mu}(\Theta) = \mu(T)/\mu(0)$ is the chemical potential normalized by the Fermi energy. Furthermore, when we are discussing wave-particle interactions, only one direction of the velocity, namely the direction that is parallel to the wave, has to be considered. Hence, we can remove the extra two dimensions by integration and then obtain the one-dimensional Fermi-Dirac distribution

$$f_{FD1}(v_\parallel) = \frac{3n}{4}\Theta \ln\left[e^{(\hat{\mu}-v_\parallel^2)/\Theta} + 1\right]. \tag{7}$$

An important difference between the quantum and the classical kinetic theory is that the distribution function of the former can take on negative values. This is because in QKT, the distribution function is defined by [13]

$$f(\boldsymbol{x}, \boldsymbol{v}) = \frac{1}{(2\pi\hbar)^3} \int d\boldsymbol{\xi} e^{-im\boldsymbol{v}\cdot\boldsymbol{\xi}/\hat{\hbar}_c} \times \left\langle \Psi^\dagger\left(\boldsymbol{x} - \frac{\boldsymbol{\xi}}{2}\right)\Psi\left(\boldsymbol{x} + \frac{\boldsymbol{\xi}}{2}\right)\right\rangle, \tag{8}$$

where $\Psi(\boldsymbol{x})$ is the quantum field operator, and $\langle\cdots\rangle$ stands for ensemble average. Equation (8) is referred to as the Wigner quasidistribution function, which can only be interpreted as a probability distribution in the classical limit. Nevertheless, the

macroscopic properties of the Wigner function are identical to the classical distribution. For example,

$$\int f(\boldsymbol{x}, \boldsymbol{v}) dv = \langle \Psi^{\dagger}(\boldsymbol{x}) \Psi(\boldsymbol{x}) \rangle = \langle n(\boldsymbol{x}) \rangle \tag{9}$$

is the average number density of the system. The dynamic behavior of the Wigner function is governed by the Wigner equation

$$(\partial_t + \boldsymbol{v} \cdot \partial_{\boldsymbol{x}}) f(\boldsymbol{x}, \boldsymbol{v}, t) = \frac{1}{i\hat{\hbar}_c} \int d\boldsymbol{\xi} \int \frac{d\boldsymbol{v}'}{(2\pi)^3} e^{i(\boldsymbol{v}'-\boldsymbol{v})\cdot\boldsymbol{\xi}/\hat{\hbar}_c} \times [\phi_+ - \phi_-] f(\boldsymbol{x}, \boldsymbol{v}', t) \tag{10}$$

in the collisionless limit. Here, $\phi_{\pm}$ is the abbreviation for $\phi(\boldsymbol{x} \pm \boldsymbol{\xi}/2)$. Along with the Poisson equation

$$-\nabla^2 \phi = 4\pi e \left[Z n_i - \int d\boldsymbol{v} f(v) \right], \tag{11}$$

where Z is the charge number of ions, the system is closed. The term "collisionless" in QKT is equivalent to the term "Hartree mean-field approximation" in DFT-based methods [15].

Noticing that if the time, coordinate, and velocity variables in the above expressions are normalized to the inverse of plasma frequency ω_p^{-1}, the Thomas-Fermi screen length $\lambda_F = v_F/\omega_p$, and the Fermi velocity $v_F = \sqrt{2\mathcal{E}_F/m_e}$, respectively, we shall replace the general NPC $\hat{\hbar}_c$ by $\hat{\hbar}_F$.

B. Numerical method

The cumbersome phase-space integration in the Wigner equation makes the numerical solution not as straightforward as that of the Vlasov equation. The first numerical approach for the Wigner equation was proposed by Suh in Ref. [27]. This approach is based on the splitting method [28], which was widely used and proven to be quite robust in solving the Vlasov equation, where the partial derivatives on the coordinate and velocity directions are treated separately. As the velocity integral of the Wigner equation can only be solved efficiently using the Fourier spectrum method (FSM), Suh's method [27] uses the FSM to advance both the coordinate and velocity direction. However, our benchmark simulations indicate that the long-time results of Suh's method are unsatisfactorily "noisy." Although there might exist some room for further improvement under Suh's pure FSM framework, we invent or adopt here an alternative numerical method: the flux balance method (FBM) [29] is used to advance the coordinate direction, and the FSM is used to advance the velocity direction. To distinguish Suh's pure FSM method, our method is referred to here as the hybrid splitting method (HSM). Benchmark simulations show that, in the case of long-time nonlinear simulations, our method, although simple, could ensure the smoothness of phase-space and energy conservation. A detailed comparison between Suh's method and our HSM method is displayed in Fig. 2.

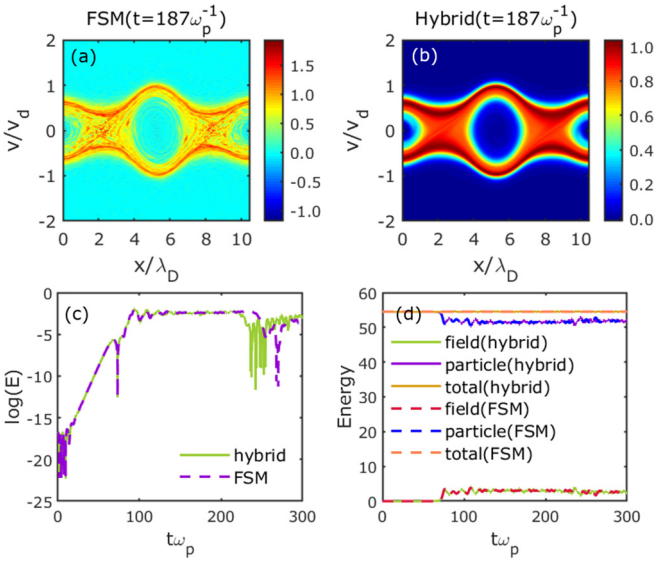

FIG. 2. Comparison between pure FSM and HSM. Parts (a) and (b) plot the phase-space snapshot of a classical BGK hole calculated by FSM and HSM, respectively. Parts (c) and (d) plot the electric field and energy of each component of the system calculated by the two methods.

III. PLASMON DECAY AND QUANTUM LANDAU DAMPING

The direct linearization of Eq. (10) yields the famous random phase approximation (RPA) [30]:

$$\epsilon(\omega, \boldsymbol{k}) = 1 + \frac{4\pi e^2}{k^2} \Pi_0(\omega, \boldsymbol{k}) = 0, \tag{12}$$

where

$$\Pi_0(\omega, \boldsymbol{k}) = \int d\boldsymbol{p} \frac{f(\boldsymbol{p}) - f(\boldsymbol{p} + \hbar\boldsymbol{k})}{\hbar\omega - \boldsymbol{k} \cdot \hbar\boldsymbol{v} - \hbar^2 k^2/2m} \tag{13}$$

is the Lindhard response function [31]. In the classical limit, where the wavelength of the collective mode is much longer than the wavelength of the electron, i.e., $|\boldsymbol{k}| \ll |\boldsymbol{p}|/\hbar$, Eq. (12) becomes

$$\epsilon(\omega, \boldsymbol{k}) = 1 - \frac{4\pi e^2}{k^2} \int d\boldsymbol{p} \frac{\boldsymbol{k} \cdot \partial_p f(\boldsymbol{p})}{\omega - \boldsymbol{k} \cdot \boldsymbol{v}}, \tag{14}$$

which is the well-known dielectric function of classical plasma. By assuming a small damping rate, the real part and the imaginary part of the Lindhard function (13) are calculated separately:

$$\mathrm{Re}[\Pi_0] = \frac{\pi}{\mathcal{E}_F \hat{k}} \mathcal{P} \int_0^{\infty} d\hat{p}\, \hat{p} f(\hat{p}) \times \left[\ln\left(\frac{\hat{p} - A_+}{\hat{p} + A_+} \right) - \ln\left(\frac{\hat{p} - A_-}{\hat{p} + A_-} \right) \right], \tag{15}$$

$$\mathrm{Im}[\Pi_0] = \frac{3\pi^2 n}{8\mathcal{E}_F k} \ln \frac{1 + \exp\left[(A_+^2 - \hat{\mu})/\Theta\right]}{1 + \exp\left[(A_-^2 - \hat{\mu})/\Theta\right]}, \tag{16}$$

where

$$A_{\pm} \equiv \hat{\hbar}_F \frac{\hat{\omega}}{\hat{k}} \pm \frac{\hat{k}}{2}, \tag{17}$$

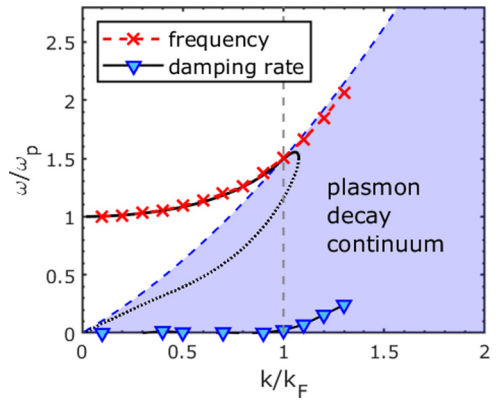

FIG. 3. Numerical result of zero-temperature ($\Theta = 0.01$) plasmon decay. The black solid line and the dotted line are calculated from Eq. (18).

and $\hat{p} = p/p_F$, $\hat{\omega} = \omega/\omega_p$, $\hat{k} = k/k_F$ are normalized quantities. As $\Theta \to 0$, an analytical result is obtained [31], i.e.,

$$\mathrm{Re}[\Pi_0] = \frac{3n}{4\mathcal{E}_F}\left[1 + \frac{k_F}{2k}(1 - A_-^2)\ln\left|\frac{1+A_-}{1-A_-}\right| - \frac{k_F}{2k}(1 - A_+^2)\ln\left|\frac{1+A_+}{1-A_+}\right|\right]. \tag{18}$$

It is clear from Eq. (15) that, when $|A_\pm| < 1$, Π_0 has no imaginary part. Thus, Eq. (12) is solved via the substitution of Eq. (18), and we plot the result in Fig. 3. The dashed line stands for a false solution from the small damping approximation. At zero temperature, there is still an electron-hole excitation continuum (the area where $|A_\pm| > 1$) in which the cold plasmons are absorbed by the electrons, although there is no Landau damping [32]. This phenomenon can be demonstrated by our linear simulation. Note that we always keep $\hat{\hbar}_F = 1$ in this section for convenience, which corresponds to a plasma with number density $n = 1.74 \times 10^{22}$ cm^{-3}.

A linear simulation result is plotted in Fig. 3, where the frequency of plasmons is represented by red crosses, and the damping rate ($-\gamma/\omega_p$) is represented by inverted triangles. One can see that the plasmons with a finite damping rate are those that fall within the plasmon decay continuum, while those that fall outside the continuum are almost identical to the Lindhard solution. From Eq. (13), we find that a plasmon when satisfying the Cerenkov condition:

$$\omega - kv - \frac{\hbar k^2}{2m} = 0, \tag{19}$$

yields a pole of the integration, which is analogous to the wave-particle resonant condition $\omega - kv = 0$ in classical plasmas. The wave-particle interaction in quantum plasmas is essentially a wave-wave interaction. Defining $q = mv/\hbar$ and $E_q = \hbar^2 q^2/2m$, then Eq. (19) becomes

$$\hbar\omega = \frac{\hbar^2(k+q)^2}{2m} - \frac{\hbar^2 q^2}{2m} = E_{k+q} - E_q. \tag{20}$$

The physical intention is rather clear: a plasmon with energy $\hbar\omega$ is absorbed by an electron with energy E_q. Figure 4(a) plots the Cerenkov match condition of a plasmon with $(\omega/\omega_p, k/k_F) = (1.58, 1.05)$. This plasmon is absorbed by an

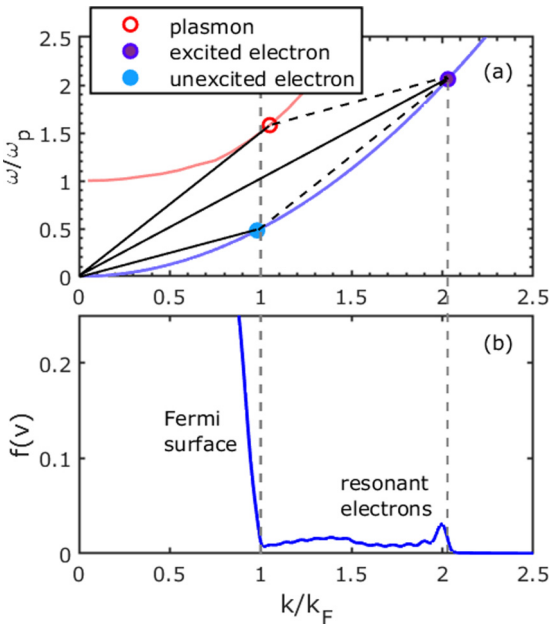

FIG. 4. This figure presents the result of plasmon decay at $k = 1.05k_F$, from which one can see that the plasmon and the electron are sitting on their dispersion relation curve correspondingly. (a) Cerenkov parallelogram matching condition. (b) Distribution function of electrons, where a small bunch of electrons are excited by plasmons.

electron slightly below the Fermi surface, and it kicks the electron out of the Fermi sea. Note that the electron obeys the dispersion relation

$$\omega = \frac{\hbar k^2}{2m}. \tag{21}$$

Actually, from Fig. 4(b) we can see that there are indeed a bunch of electrons excited to the corresponding location. However, such a high-energy electron beam may not always be observed, especially in higher-wave-number cases, due to nonlinear phase mixing or quantum correlation.

As the temperature rises, the role of the thermal Landau damping begins to emerge. To obtain the exact solution of Eq. (12), we need to extend the domain of the definition of ω to the region where $\mathrm{Im}[\omega] < 0$ by means of analytic continuation, i.e.,

$$\Pi_0(\omega, \boldsymbol{k}) = \begin{cases} \int dv_\parallel \frac{f^-_{\mathrm{FD1}} - f^+_{\mathrm{FD1}}}{\hbar\omega - k\hbar v_\parallel}, & \mathrm{Im}[\omega] > 0, \\ \int dv_\parallel \frac{f^-_{\mathrm{FD1}} - f^+_{\mathrm{FD1}}}{\hbar\omega - k\hbar v_\parallel} & \\ \quad + \frac{2\pi i}{\hbar}[f^-_{\mathrm{FD1}} - f^+_{\mathrm{FD1}}]_{v_\parallel = \frac{\omega}{k}}, & \mathrm{Im}[\omega] < 0, \end{cases} \tag{22}$$

where $f^\pm_{1\mathrm{FD1}} = f^\pm_{1\mathrm{FD1}}(p_\parallel \pm \hbar k/2)$, and the extra term in the $\mathrm{Im}[\omega] < 0$ region comes from the residue of the integrand at the pole, $v_\parallel = \omega/k$. In Fig. 5, we calculated $\Theta = 0.2$, 1, and 2, which correspond to $T = 5672$, 28 360, and 56 720 K, respectively, in an $\hat{\hbar}_F = 1$ plasma. These parameters roughly fall within the parameter range of WDM experiments [2,33]. Similar results were obtained by Ref. [34], in which the

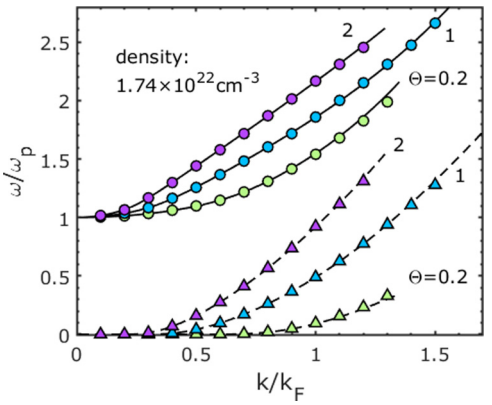

FIG. 5. Linear Landau damping of a dense ($\hat{\hbar}_F = 1$) plasma. The solid lines and the dashed lines are the real part and the negative of the imaginary part, respectively, of the exact solutions of Eq. (12), while the circles and the triangles are the corresponding simulation results.

authors adopted a PIC semiclassical simulation and did not include the quantum recoil effect.

IV. QUANTUM TWO-STREAM INSTABILITY AND THE QUANTUM BGK MODE

A. Linear result

Two-stream instability in quantum plasmas has been investigated by many authors [35–39]. However, despite the fact that two-stream instability is a reactive-type instability, i.e., the instability is driven by the Hermitian part of the dielectric function [40], the real-world plasma always possesses finite temperature. Especially in a high-density plasma, the Pauli exclusive principle ensures that the electrons have finite velocities even at zero temperature. Thus, regardless of the reliability of QHD, a kinetic method is needed, as is pointed out in Refs. [35,38].

In the fluid limit, it is convenient to define another NPC:

$$\hat{\hbar}_d = \hbar\omega_p/mv_d^2, \tag{23}$$

where v_d is the relative drift velocity of the two streams. Hence the eigenmode frequency of quantum fluid two-stream instability can be written as [38,41]

$$\omega = \frac{\omega_p}{\sqrt{2}}\left[1 + 2\hat{\hbar}_d\tilde{k}^2 + \frac{\hat{\hbar}_d^2\tilde{k}^4}{2} \pm \sqrt{1 + 8\tilde{k}^2 + 4\hat{\hbar}_d^2\tilde{k}^6}\right]^{\frac{1}{2}}, \tag{24}$$

where $\tilde{k} = kv_d/\omega_p$. As is shown in the left panel of Fig. 6, the quantum recoil effect creates an extra unstable region that hides itself at $k = \infty$ when $\hat{\hbar}_d = 0$. As $\hat{\hbar}_d$ increases, this unstable quantum "bubble" moves toward a longer wavelength and is absorbed by the original unstable bubble at a certain value of $\hat{\hbar}_d$. Notice that the quantum bubble is always located in a relatively high-wave-number region, where any disturbance is heavily Landau-damped. As a result, this unstable region may not exist in real dense plasma. In the right panel of Fig. 6, we simulated a quantum two-stream instability around $\hat{\hbar}_d = 1$ with an exaggerated drift velocity, i.e., $v_d = 50v_F$, in order to eliminate the kinetic effect. Even so, the numerical approach still cannot reproduce the quantum bubble calculated by Eq. (24), except for some distortion in the high-wave-number region.

We will show in the next sections that the quantum effect has the most impact in the nonlinear phase by considering a more realistic quantum plasma with a reasonable ratio of Fermi velocity to drift velocity.

B. BGK equilibrium in a weak quantum system

It is shown by Bernstein, Green, and Kruskal [42] that there exists a nonlinear equilibrium mode, namely the BGK mode, in an electron electrostatic plasma. The BGK mode is ubiquitous in the field of plasma physics because it provides an important kinetic nonlinear saturation mechanism for many plasma instabilities. The onset of particle trapping in quantum Landau damping is briefly discussed in Ref. [34], where the potential trough that traps the particle is rather shallow because this trapping process occurs after a period of Landau damping. Here, we set up a BGK equilibrium with a symmetrical electron two-stream system to investigate the particle trapping process in quantum plasma. To see how the quantum recoil effect affects the BGK mode, we scan the NPC $\hat{\hbar}_T$ from 0 (Vlasov equation) to 10. As $\hat{\hbar}_T$ increases, which means that the temperature decreases and the density increases, the

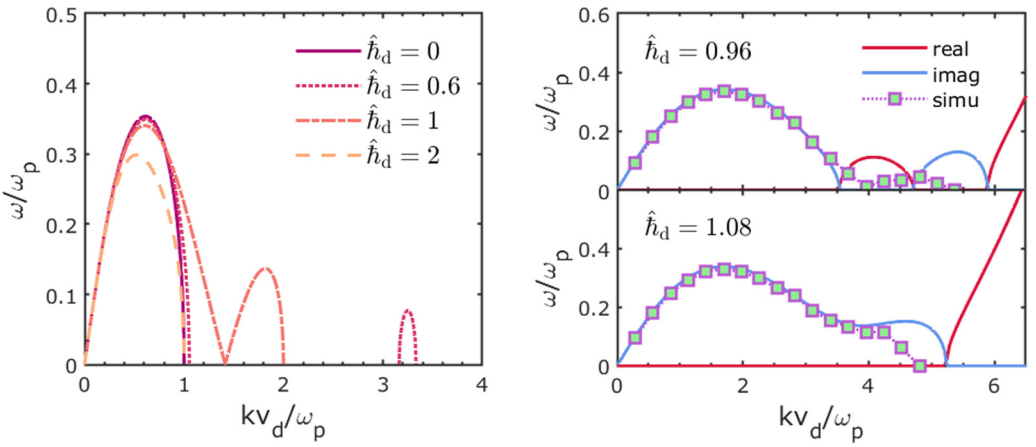

FIG. 6. Dispersion relation of quantum two-stream instability varying with $\hat{\hbar}_d$ (left). Simulation of the extra unstable region created by the quantum recoil effect (right).

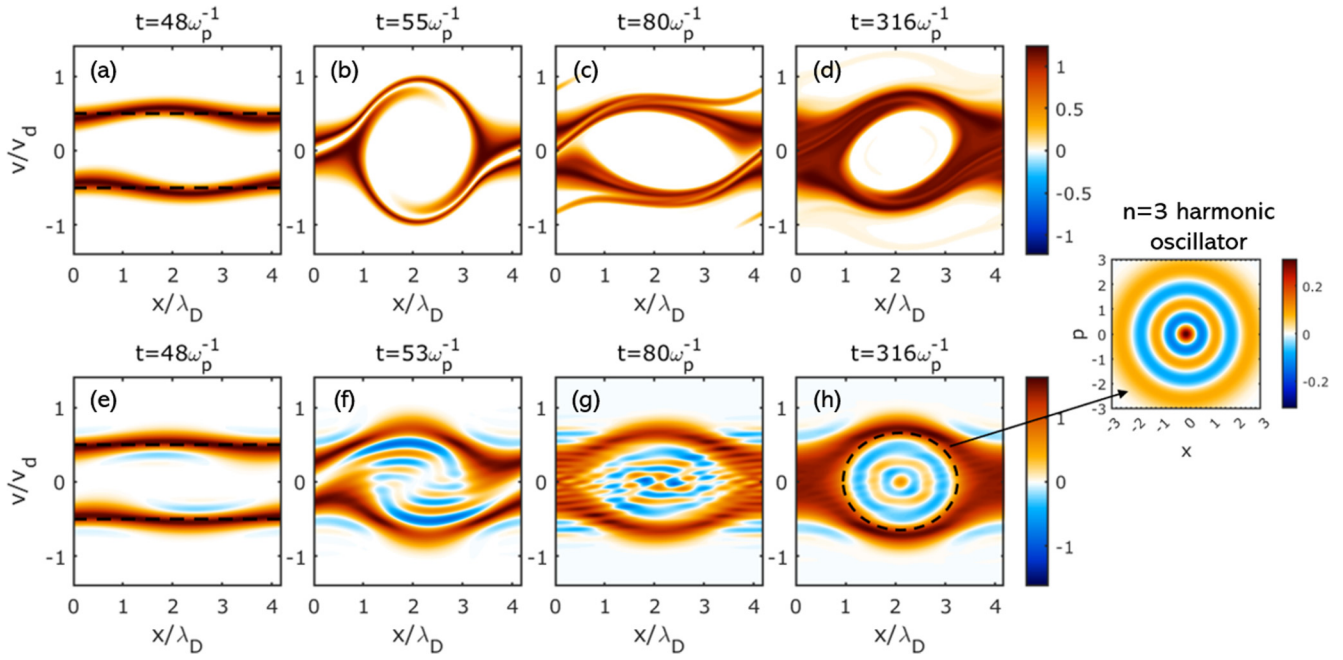

FIG. 7. (a)–(d) BGK equilibrium in classical plasma. (e)–(h) BGK equilibrium in weak quantum plasma; an $n = 3$ quantum oscillator is formed at the nonlinear stage.

quantum recoil effect will eventually become dominant, and the kinetic effect disappears. A system in the state in which kinetic effects completely disappear is referred to as a strong quantum system, and the medium state between quantum and classical systems is called a weak quantum system.

The snapshots of typical moments of the development of a classical BGK mode are presented in the upper panels of Fig. 7. Panel (a) stands for the end of linear growth, and the electron beams start to twist. In panel (b), electrons with velocity near the wave velocity (which is equal to zero in our wave frame of reference) bounce off the potential barrier and complete a full cycle at panel (c). A nearly steady state is formed after several bounce periods, as is shown in panel (d).

In the lower panel of Fig. 7, where $\hat{\hbar}_{\mathrm{T}} = 0.8$, one can see that, from panels (e)–(h), the basic shape of a classical BGK hole is preserved. This is a typical weak quantum system. Consider a pure-state harmonic oscillator, the Wigner representation of which is [43]

$$w_n(x, p) = \frac{1}{\pi}\left(\frac{1}{4}\right)^n e^{-(x^2+p^2)} \sum_{k=0}^{n} \frac{H_{2k}(\sqrt{2}x)H_{2(n-k)}(\sqrt{2}p)}{k!(n-k)!}, \tag{25}$$

where H_n is the nth-order Hermitian function, and thus n is the quantum number of a quantum harmonic oscillator. The pictorial representation of Eq. (25) is a ripplelike structure, which is exactly like what we have found in the nonlinear saturation phase of the $\hat{\hbar}_{\mathrm{T}} = 0.8$ quantum BGK mode, as is shown in Fig. 7(d). The physical interpretation is rather clear: the hollow structure in the classical BGK mode is merely the phase-space representation of a classical oscillator, hence it is not surprising to find a quantum oscillator in a quantum BGK mode.

C. Periodic solution in a strong quantum system

We examine a strong quantum system further by increasing the product of the NPC $\hat{\hbar}_{\mathrm{F}}$ and wave number $\hat{k}$, which indicates the ratio of energy and momentum between a plasmon and an electron sitting on the Fermi surface. The energy of the resonant mode of three typical parameters is presented in Fig. 8, from which we found that when $\hat{\hbar}_{\mathrm{F}}\hat{k} = 2$ the wave energy is almost constant in the nonlinear saturation phase, and this is corresponding to the quantum BGK equilibrium we have discussed in the previous section. When the value of $\hat{\hbar}_{\mathrm{F}}\hat{k}$ is high enough, one can see that an interesting phenomenon occurs at the nonlinear phase: when the electric potential reaches its linear limitation, instead of saturating into a relatively steady state, the wave damps to equilibrium level with the damp rate exactly equal to the opposite of the linear growth rate, and then it grows back to the linear limitation, and so on and so forth. This nearly periodic anomalous oscillation does not fade away after hundreds of plasma

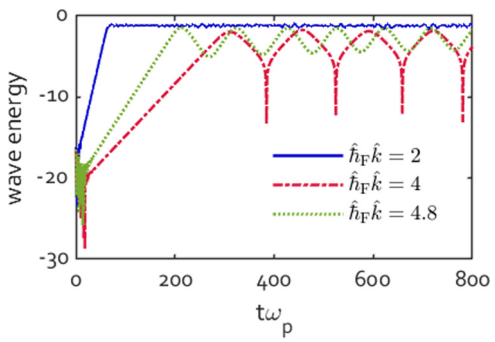

FIG. 8. Energy evolution of two-stream instability with different values of $\hat{\hbar}_{\mathrm{F}}\hat{k}$.

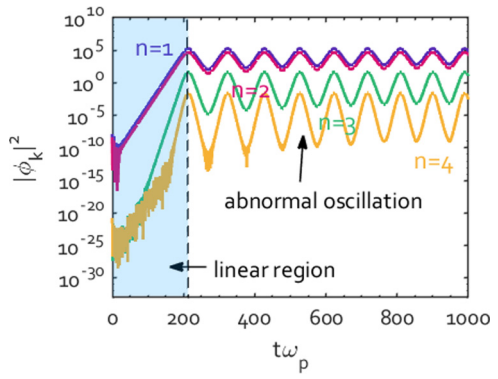

FIG. 9. Abnormal oscillation of an $\hat{\hbar}_F\hat{k} = 4.8$ quantum two-stream instability; the harmonics grow and damp with its corresponding linear growth rate.

oscillation periods if there is no dissipation mechanism. The evolution of the harmonics of the $\hat{\hbar}_F\hat{k} = 4.8$ electric potential is plotted in Fig. 9. Notice that this intriguing phenomenon is quite analogous with what is reported in Ref. [41] by means of the quantum Dawson model, i.e., a coupled Schrödinger-Poisson model. The quantum Dawson model is approximately equivalent to the Wigner-Poisson model, when the number of pure states N is large enough.

The abnormal oscillation results from the energy exchange between electrons and the plasmon. The momentum of the plasmon, i.e., the wave number of the quantum Langmuir wave, must obey the condition

$$\hat{\hbar}_F\hat{k} \gtrsim \hat{v}_d - 2, \tag{26}$$

or, equivalently,

$$\frac{\hbar k}{m} \gtrsim \frac{1}{2}(v_d - 2v_F). \tag{27}$$

This condition is not exact because there are always thermal electrons outside of the Fermi surface when the temperature is finite. As shown in Fig. 10, the drift velocity of the two electron beams is $6v_F$, thus the normalized momentum of a plasmon $\hat{\hbar}_F\hat{k}$ should be approximately larger than 4. Panel (a) is a classical BGK equilibrium, while panel (b) is a quantum BGK equilibrium where the wavelength of the resonant mode does not satisfy the threshold condition (26), hence there the abnormal oscillation does not occur. On the contrary, in panels (c) and (d), while the velocity distribution at the peak of the abnormal oscillation is plotted, we find that a pair of electron bunch are excited according to the Cerenkov condition (19). Thus, this abnormal oscillation stems from the wave-wave energy exchange, which is the quantum version of the wave-particle energy exchange mechanism in classical plasma physics.

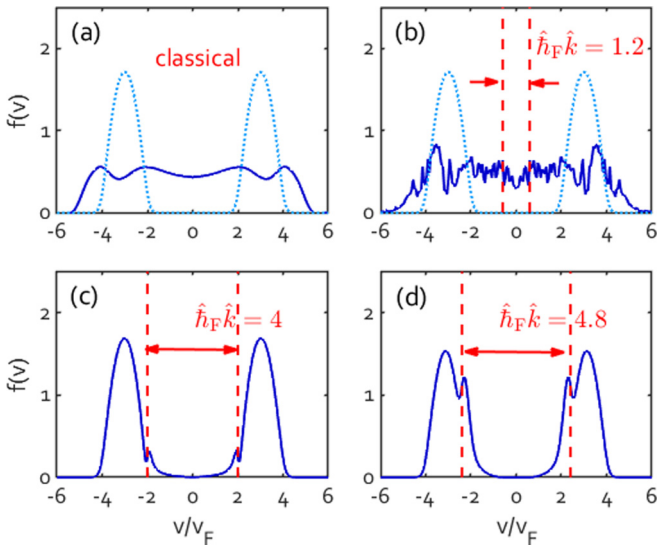

FIG. 10. Velocity distribution of (a) classical BGK equilibrium, (b) quantum BGK equilibrium, and (c),(d) the peak of the abnormal oscillation. The dotted-line stands for the initial distribution.

V. CONCLUSION AND DISCUSSION

In this paper, the Wigner-Poisson system is solved numerically by using a hybrid numerical scheme in order to investigate the quantum nature of dense plasmas. Our hybrid numerical scheme, though simple, shows significant advantages in energy conservation and smoothness of phase space. The linear results of simulations are benchmarked with RPA theory. The thermal effect on linear quantum Landau damping is also benchmarked by both the eigenvalue method and the time-dependent initial value method, which show almost identical results.

In the nonlinear region, the role of the quantum recoil effect in dense plasma is studied in detail. The BGK equilibrium formed by two counterflowing electron beams demonstrates an interesting yet perspicuous quantum-mechanical phenomenon. When the wavelength of the wave function of an electron is much shorter than the wavelength of the collective mode but still long enough such that the wave effect cannot be ignored, the electrons trapped in the potential trough form a quantum oscillator in phase space. When the scale of the two wavelengths is comparable and a threshold condition is satisfied, the energy exchange between the electron and the collective mode results in an abnormal oscillation that does not exist in classical plasmas.

ACKNOWLEDGMENTS

This work was supported by the National Natural Science Foundation of China (Grants No. 11875235, No. 61627901, No. 12075204), and the Strategic Priority Research Program of Chinese Academy of Sciences (Grant No. XDA250050500). D.W. thanks the sponsorship from Yangyang Development Fund.

[1] G. Manfredi, Fields Inst. Commun. **46**, 263 (2005).

[2] S. H. Glenzer, O. L. Landen, P. Neumayer, R. Lee, K. Widmann, S. W. Pollaine, R. J. Wallace, G. Gregori, A. Höll, T. Bornath *et al.*, Phys. Rev. Lett. **98**, 065002 (2007).

[3] P. K. Shukla and L. Stenflo, Phys. Plasmas **13**, 044505 (2006).

[4] A. C. Hayes, M. E. Gooden, E. Henry, G. Jungman, J. B. Wilhelmy, R. S. Rundberg, C. Yeamans, G. Kyrala, C. Cerjan, D. L. Danielson *et al.*, Nat. Phys. **16**, 432 (2020).

[5] J. Daligault and S. Gupta, Astrophys. J. **703**, 994 (2009).

[6] T. Dornheim, S. Groth, and M. Bonitz, Phys. Rep. **744**, 1 (2018).

[7] P. Hohenberg and W. Kohn, Phys. Rev. **136**, B864 (1964).

[8] W. Kohn and L. J. Sham, Phys. Rev. **140**, A1133 (1965).

[9] C. Gao, S. Zhang, W. Kang, C. Wang, P. Zhang, and X. T. He, Phys. Rev. B **94**, 205115 (2016).

[10] S. Zhang, H. Wang, W. Kang, P. Zhang, and X. He, Phys. Plasmas **23**, 042707 (2016).

[11] S. Zhang, S. Zhao, W. Kang, P. Zhang, and X.-T. He, Phys. Rev. B **93**, 115114 (2016).

[12] E. Wigner, Phys. Rev. **40**, 749 (1932).

[13] L. P. Kadanoff, *Quantum Statistical Mechanics* (Benjamin, Boca Raton, 1962).

[14] D. Kremp, T. Bornath, M. Bonitz, and M. Schlanges, Phys. Rev. E **60**, 4725 (1999).

[15] G. Manfredi, P.-A. Hervieux, and J. Hurst, Rev. Mod. Plasma Phys. **3**, 13 (2019).

[16] J.-H. Liang, T.-X. Hu, D. Wu, and Z.-M. Sheng, Phys. Rev. E **105**, 045206 (2022).

[17] B. Hao, W. Ding, Z. Sheng, C. Ren, X. Kong, J. Mu, and J. Zhang, Phys. Plasmas **19**, 072709 (2012).

[18] D. Wu, W. Yu, S. Fritzsche, and X. T. He, Phys. Rev. E **102**, 033312 (2020).

[19] G. Manfredi and F. Haas, Phys. Rev. B **64**, 075316 (2001).

[20] L. G. Garcia, F. Haas, L. P. L. De Oliveira, and J. Goedert, Phys. Plasmas **12**, 012302 (2005).

[21] P. K. Shukla and B. Eliasson, Phys. Rev. Lett. **96**, 245001 (2006).

[22] D. Shaikh and P. K. Shukla, Phys. Rev. Lett. **99**, 125002 (2007).

[23] P. K. Shukla and B. Eliasson, Phys. Rev. Lett. **108**, 165007 (2012).

[24] M. Bonitz, E. Pehlke, and T. Schoof, Phys. Rev. E **87**, 033105 (2013).

[25] M. Bonitz, Z. A. Moldabekov, and T. S. Ramazanov, Phys. Plasmas **26**, 090601 (2019).

[26] G. Brodin, J. Zamanian, and J. Mendonca, Phys. Scr. **90**, 068020 (2015).

[27] N.-D. Suh, M. R. Feix, and P. Bertrand, J. Comput. Phys. **94**, 403 (1991).

[28] C.-Z. Cheng and G. Knorr, J. Comput. Phys. **22**, 330 (1976).

[29] F. Filbet, E. Sonnendrücker, and P. Bertrand, J. Comput. Phys. **172**, 166 (2001).

[30] D. Pines and D. Bohm, Phys. Rev. **85**, 338 (1952).

[31] J. Lindhard, Dan. Vid. Selsk Mat.-Fys. Medd. **28**, 8 (1954).

[32] V. S. Krivitskii and S. V. Vladimirov, Sov. J. Exp. Theor. Phys. **73**, 821 (1991).

[33] R. Roycroft, P. A. Bradley, E. McCary, B. Bowers, H. Smith, G. M. Dyer, B. J. Albright, S. Blouin, P. Hakel, H. J. Quevedo, E. L. Vold, L. Yin, and B. M. Hegelich, Matter Radiat. Extremes **6**, 014403 (2021).

[34] J. Daligault, Phys. Plasmas **21**, 040701 (2014).

[35] S. Son, Phys. Lett. A **378**, 2505 (2014).

[36] F. Haas and B. Eliasson, Phys. Scr. **90**, 088005 (2015).

[37] A. Bret and F. Haas, Phys. Plasmas **17**, 052101 (2010).

[38] J.-H. Liang, T.-X. Hu, D. Wu, and Z.-M. Sheng, Phys. Rev. E **103**, 033207 (2021).

[39] F. Haas, A. Bret, and P. K. Shukla, Phys. Rev. E **80**, 066407 (2009).

[40] L. Chen, *Waves and Instabilities in Plasmas* (World Scientific, Singapore, 1987), Vol. 12.

[41] F. Haas, G. Manfredi, and M. Feix, Phys. Rev. E **62**, 2763 (2000).

[42] I. B. Bernstein, J. M. Greene, and M. D. Kruskal, Phys. Rev. **108**, 546 (1957).

[43] Y.-S. Kim and M. E. Noz, *Phase Space Picture of Quantum Mechanics: Group Theoretical Approach* (World Scientific, Singapore, 1991), Vol. 40.